Naya, F., Herráez, M., Lopes, C., González, C., van der Veen, S. & Pons, F. (2017). Computational micromechanics of fiber kinking in unidirectional FRP under different environmental conditions. *Composites Science and Technology, 144*, 26–35.

DOI: 10.1016/j.compscitech.2017.03.014

Computational micromechanics of fiber kinking in unidirectional FRP under different environmental conditions

F. Naya[a], M. Herráez[a], C.S. Lopes[a,*], C. González[a,b], S. Van der Veen[c], F. Pons[c]

[a]*IMDEA Materials Institute, C/Eric Kandel, 2, 28906 Getafe, Madrid, Spain*
[b]*Department of Materials Science, Polytechnic University of Madrid, ETS de Ingenieros de Caminos, 28040 Madrid, Spain*
[c]*AIRBUS Structures Research and Integration, ESIRNM. 18 rue Marius Terce, 31300 Toulouse, France*

Abstract

The determination of ply properties of Fiber Reinforced Polymers (FRP) for particular operational environmental conditions in aeronautical applications is mandatory in order to fulfill current industry stringent certification requirements. However, the traditional experimental approach requires massive investments of resources and time. From the behaviour obtained experimentally, constitutive equations including failure criteria are then devised to be used in the design of FRP structures. The ply longitudinal behaviour under compression is generally the most difficult to measure and characterize. In this work, an alternative coupled experimental-computational micromechanics approach is proposed to determine the longitudinal compression properties of unidirectional FRP plies under different environmental conditions. This methodology includes experimental characterization of matrix and fiber/matrix interface, combined with numerical simulations of realistic microstructures. The interface decohesion is simulated using cohesive-frictional interactions. A pressure dependent, elastoplastic model that includes tensile damage is employed to capture the matrix nonlinear behavior. The numerical predictions match the experimentally-obtained ply properties available in the literature in a remarkable way and suggest that virtual ply property characterization is a mature and reliable approach to conduct screening of materials.

Keywords: A. Polymer-matrix composites (PMCs), C. Multiscale modeling, C. Finite element analysis(FEA), C. Computational micromechanics

*Corresponding author
Email address: claudiosaul.lopes@imdea.org (C.S. Lopes)

1. Introduction

Fiber Reinforced Polymers (FRP's) are nowadays extensively used in applications where very good mechanical properties are required in combination with weight savings. In most cases, the specific longitudinal properties are their best selling point, and fast ways to determine those constitute an advantage in the process of design of composites. Up to date, various phenomenological as well as physically-based models have been proposed for unidirectional (UD) composites [1]. However, their input parameters need to be obtained through costly and time-consuming experimental campaigns. This is the case of certification in the aeronautical industry where the whole process for each material can last well over a year due to the required tests for different environmental and ageing conditions.

Under longitudinal compression, ply failure is triggered by the mechanism of fiber kinking, a damage mode that is strongly affected not only by the elastic properties of the fibers but also by their geometry (waviness, diameter, shape, etc.) [2, 3, 4, 5]. In the present work, the effects of variation in fiber shape and diameter was not studied because the geometry of the material constituent fibers were found to be very homogeneous. Moreover, void content [6, 7] and other imperfections (crushed fibers) arising from the manufacturing process were also found to affect the kinking phenomenon [8, 9] but these are also out of the scope of the present investigation.

The prediction of the longitudinal compression strength has been tackled by both analytic [2, 3, 10] and numeric approaches [11, 4, 5, 12, 13] that simulate the complex fiber kinking mechanism with more or less detail and accuracy. In the case of numerical simulation, models are usually based on two-dimensional micromechanical RVE's and assume perfect hexagonal fiber packing arrangements. One recent exception, allowed by the increasingly available computational resources, is the work of Bai et al. [14] that provided micro-scale evidence supporting the hypothesis that shear stresses transferred between fibers and matrix are particularly important in the formation of the kink band. However the effects of fiber distribution, polymer plasticity and damage as well as that of the fiber/matrix debonding and friction, in the kink-band initiation and propagation are still unclear.

Computational micromechanics based on Finite Element Analyses (FEA) offers a reliable and efficient methodology to simulate the deformation and fracture mechanisms of engi-

neering materials. Numerical simulations of Representative Volume Elements (RVE) of the composite microstructure are able to predict ply properties, in good agreement with experimental data, e.g. [15, 16, 17], providing input data for mesomechanical models that can then be used in the analysis of laminates.

The aim of this work is to develop a reliable and accurate computational approach supported by micromechanical *in situ* measurements of the material constituents to predict the longitudinal compression mechanical properties of a composite ply (stiffness and strength) under different operating environmental conditions. In a previous work, the authors applied this strategy to study the transverse and shear behaviors of UD composites [15]. This bottom-up analysis approach enables, among many possibilities, the in-situ virtual testing of specific regions of the ply, the fast characterization of different combinations of matrices and fibers, the study of micro-defects resulting from deficient curing conditions [18]. This leads to the reduction of time and costs involved in new material designs and provides fast screening capabilities that improve material selection in engineering applications.

Following the approach of other authors [2, 4, 10, 12], the initial fiber misalignment angle (ϕ_0), is assumed to control the compressive failure of the ply by triggering fiber kinking. A three-dimensional numerical approach, that includes a coupled plasticity-damage model for the matrix and a cohesive-frictional behavior for the fiber/matrix interface, is used to investigate the influences of statistically representative microstructures and constituent mechanical properties on the longitudinal compression response of the AS4/8852 composite ply. The behavior of the microconstituents is modeled based on in-house characterization by means of in-situ micromechanical tests, and the resulting properties are directly used as inputs of the constitutive equations of fibers, matrix and interfaces that are available in the FE software package ABAQUS [19] without the need of user subroutines, in what constitutes a great advantage for the broad use of the proposed approach. Detailed intra-ply information (fiber diameter distribution, volume fraction, fiber clusters and resin pockets) is captured and included in the computational model, as in previous works [20, 15]. The prediction of ply properties is obtained by homogenizing the simulated response of the periodic RVE to longitudinal compression loads.

To model the initial imperfection, the models developed in this work contain sinusoidal

shaped fibers and allow the prediction of the sensitivity function, $X_C(\phi_0)$, that represents the evolution of the longitudinal compression strength, X_C, for different values of ϕ_0. Additionally, an initial fiber misalignment probability density, $f(\phi_0)$, is considered to achieve an objective prediction of the ply strength.

This introduction is followed by the description of the computational micromechanics framework, i.e. of the constitutive equations used to simulate matrix, fiber and interfaces, as well of the RVE generation procedure and the subsequent construction of the FE models with the specific loading conditions. Then, the results of the pure compression loading simulations performed on one material case (Hexcel carbon/epoxy AS4/8552 material, with 60% fiber volume fraction and 0.184 mm cured ply thickness) are presented and correlated with reliable experimental results available in the literature [21]. After a discussion to the methodology and results is presented, a conclusion to this work is given.

2. Computational micromechanics for compression of unidirectional plies

2.1. Initial fibre misalignment distribution

The initial fiber misalignment distribution was taken from Czabaj et al. [22], who reproduced the realistic three-dimensional fiber distribution of AS4/3501-6 plies using high resolution images obtained by means of X-ray computed tomography. The material used by Czabaj et al. is very similar to the AS4/8552 material system used in the present work and, hence, his misalignment probability density function is used here without further modifications (see Figure 1). Although X-ray computed tomography is very time-consuming, this method is still faster than the alternative one proposed by Yurgartis [23], which consists in calculating the real (elliptic) cross section of several fibers on selected micrographs and compare these measurements against the ideal (circular) ones to obtain the rotation of the fiber section and, therefore the misalignment angle. Yugartis' method was demonstrated to provide reproducible results [24]. However, it is extremely time consuming because the area of individual fibers is obtained by means of direct observation of individual micrographs captured from selected cross sections of the composite, involving cutting, polishing and extensive observation work.

The fiber misalignment sensitivity function, $X_C(\phi_0)$, is expected to be symmetric with respect to the sign of the initial fiber misalignment ϕ_0. However, the fiber misalignment distribution function $f(\phi_0)$ devised by Czabaj et al.[22] is clearly not symmetric, probably due a limited amount of observations. To overcome this issue, the half-function corresponding to negative misalignment (ϕ_0^-) is folded around the vertical axis (see Figure 1). The resulting probabilities $f(-\phi_0^-)$ are averaged with the half-function $f(\phi_0^+)$ values corresponding to positive misalignment. Then, the symmetric $\bar{f}(\phi_0)$ can be fitted by a Gaussian function, $\bar{f}_G(\phi_0)$, valid for the whole range of angles, which in turn is directly integrated to obtain the corresponding symmetric fiber misalignment cumulative density function, $F(\phi_0)$ (Figure 1).

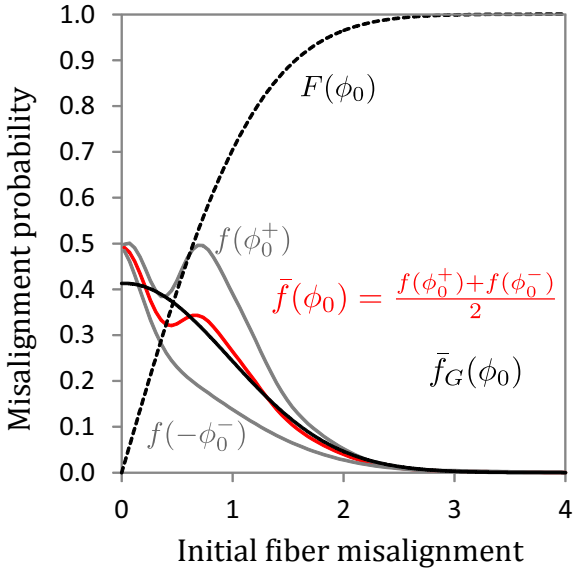

Figure 1: Initial AS4 fiber misalignment distributions, $f(\phi_0^+)$ and $f(-\phi_0^-)$, extracted from [22]. Gaussian fiber misalignment probability density function, $\bar{f}_G(\phi_0)$, and cumulative density function, $F(\phi_0)$, resulting from fitting the symmetric $\bar{f}(\phi_0)$ probability function

2.2. Set-up and simulation of the 3D RVE models

The computational micromechanics framework is based on the analysis of a statistically representative volume element of the material (RVE) subjected to homogeneous stress states (tension, compression and shear) or temperature increments. The microstructure of the RVE of a unidirectional composite was idealized as a random dispersion of parallel and circular fibers in the polymer matrix. A modeling domain encompassing around 50 fibres was found large enough to capture adequately the essential features of the microstructural

behaviour [25]. Synthetic fiber distributions statistically equivalent to the real ones were generated for the analysis using the Random Sequential Adsorption (RSA) algorithm [26]. Two-dimensional periodic fiber distributions embedded in resin matrix were extruded along the fiber direction to achieve the final RVE's of the unidirectional composite material which were then discretized using fully integrated isoparametric linear wedge (C3D6) and brick (C3D8) finite elements to model fibers and matrix. Periodic boundary conditions were applied on opposite faces of the RVE's in three dimensions, according to the methodology developed by Segurado and LLorca [26].

In order to capture the influence of the initial fibre misalignment angle in the formation of the kink band, the total length of the RVE was set equal to one half of the wavelength associated to the sinusoidal function used to model the initial shape of the fiber (Figure 2). For carbon fibers, a value $W = 500\,\mu\text{m}$ was adopted following other authors [12, 13]. As a consequence of the large RVE size the model resulted in around 1.2 million DOF's, including internal variables generated to tackle the contact interactions associated to fiber/matrix interfaces. Simulations were carried out using ABAQUS [19] within the framework of the finite deformations theory taking into account residual thermal stresses generated during cool-down from the composite process temperature. The nonlinear problem was solved incrementally by means of the Newton-Raphson method using implicit integration (Abaqus/Standard). The model took over 72 hours to compute using an HPC cluster of 40 Intel Xeon E5-2670 cores and GPU acceleration.

The multi-fibre model resulted impractical to evaluate the sensitivity function $X_{\text{C}}(\phi_0)$. To improve efficiency, a simplified RVE model of a single fiber containing only ≈ 100 thousand DOF's was developed, as shown in Figure 3. This single-fibre RVE contains the same fiber volume fraction as the multi-fibre one, but resulted in a reduction of the computational time to less than an hour using similar computational resources. This RVE size is convenient to perform parametric analyses and obtain an approximated $X_{\text{C}}(\phi_0)$ response.

Since the carbon fiber was modeled as an elastic transversely isotropic material, a local material orientation was required. To this end, the geometry of the fibers was partitioned and the resulting portions were oriented using the tangent direction corresponding to the sinusoidal-generation function at the the center of each fiber fragment. To avoid spurious

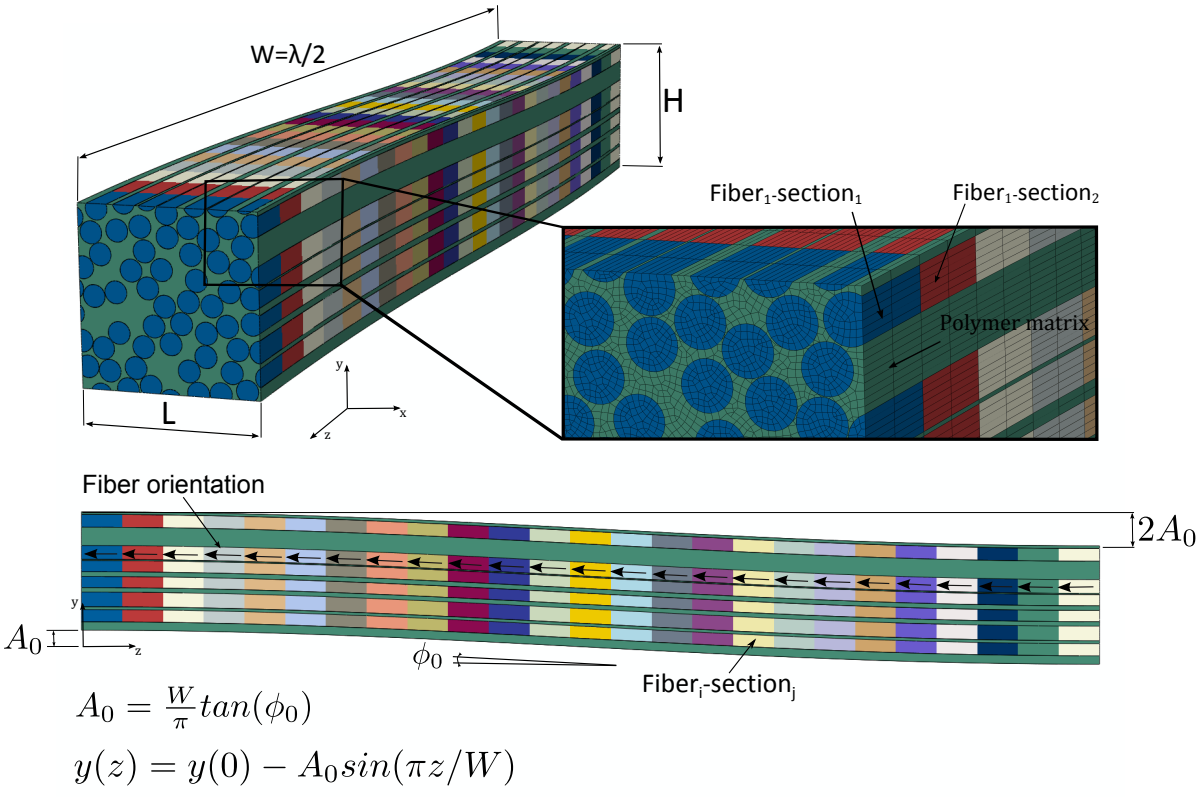

Figure 2: Multi-fibre FE model used in the simulation of longitudinal compression of a AS4/8552 ply. Each color represents one section. The arrows show the orientation of the fibers

element deformation modes and shear locking that would lead to numerical problems and inaccurate predictions of $X_{\mathrm{C}}(\phi_0)$, it is convenient that these partitions are made using planes perpendicular to the local fiber axis instead of the global longitudinal axis. In other words, these partition planes correspond with the plane of transverse isotropy of the fibers and their orientation changes according to the sinusoidal function used to generate the model.

2.3. Material models of the RVE constituents

The carbon fibers were modeled as linear elastic and transversely isotropic solids defining five independent elastic constants (E_{f1}, E_{f2}, ν_{f12}, G_{f12}, G_{f23}) and two different thermal expansion coefficients (α_{f1}, α_{f2}).

The polymer matrix was simulated as an isotropic linear and elastic solid being E_{m} and ν_{m} its elastic modulus and Poisson ratio, respectively. The model allows the resin to undergo plastic deformation with the possibility of damage by cracking under tensile loads. This approach has been demonstrated to represent a realistic behavior of a composite polymer

resin [15]. This coupled damage-plasticity model, available in ABAQUS [19], is a modification of the Drucker-Prager plasticity yield surface [27] by including a damage variable in order to capture the quasi-brittle behaviour of the polymer under dominant tensile loads. The constitutive equation is based on the yield function proposed by Lubliner et al. [28] and includes modifications proposed by Lee and Fenves [29] to account for strength evolution under tension and compression loads. After the onset of damage in tension, the softening behavior is controlled by an exponential cohesive law, characterized by a single normalized scalar damage variable, to ensure the correct rate of matrix energy release. Details of this constitutive model and of the numerical implementation can be found in [16, 15, 19].

The debonding between fibers and matrix was modeled by means of a classical cohesive zone method coupled with frictional behavior. The constitutive equation that couples both phenomena relates the displacement jump vector across the interface (Δ) to the traction vector acting on it (τ) by means of a single normalized scalar damage variable (d) to simulate delamination and friction under the full range of modes (normal - τ_{N}, shear transversal - τ_{T}, and shear longitudinal - τ_{L})) and mode mixities:

$$\tau = \left\{ \begin{array}{c} \tau_{\mathrm{T}} \\ \tau_{\mathrm{L}} \\ \tau_{\mathrm{N}} \end{array} \right\} = (1-d)K \left\{ \begin{array}{c} \Delta_{\mathrm{T}} \\ \Delta_{\mathrm{L}} \\ \Delta_{\mathrm{N}} \end{array} \right\} - dK \left\{ \begin{array}{c} 0 \\ 0 \\ \langle -\Delta_{\mathrm{N}} \rangle \end{array} \right\} + \mu dK \left\{ \begin{array}{c} \langle -\Delta_{\mathrm{N}} \rangle \frac{\Delta_{\mathrm{T}}}{\Delta_{\mathrm{S}}} \\ \langle -\Delta_{\mathrm{N}} \rangle \frac{\Delta_{\mathrm{L}}}{\Delta_{\mathrm{S}}} \\ 0 \end{array} \right\} \qquad (1)$$

wherein $\Delta_{\mathrm{S}} = \sqrt{{\Delta_{\mathrm{T}}}^2 + {\Delta_{\mathrm{L}}}^2}$, and K is a scalar penalty contact stiffness that describes the linear-elastic behaviour of the interface prior to damage initiation, and under any compressive normal tractions which are assumed not to cause damage to the interface ($\langle x \rangle = max(0, x)$). Coulomb-type friction is introduced by the coefficient μ. The penalty stiffness K is a non-physical numerical parameter that should be large enough to ensure displacement continuity in the absence of interface damage while avoiding convergence difficulties due to ill-conditioned stiffness matrix.

In ABAQUS [19], this cohesive-frictional behaviour is coupled with a surface contact interaction algorithm. This approach was used in this work to model the coupled effects of fibre/matrix friction and debonding. In this way, the shear stresses caused by friction at the interface are ramped progressively and proportional to the degradation of the interface, thus

once the interface is fully debonded, the surface interaction is uniquely governed by a pure Coulomb model, $\tau_{\mathrm{T,L}} = \mu K \langle -\Delta_{\mathrm{N}} \rangle$. Furthermore, friction also affects the cohesive response as frictional stresses are ramped with the interface cohesive damage variable. This causes an increase of the interface shear resistance that is function of the normal compressive tractions applied on it.

For the pure cohesive response, damage onset is controlled by a quadratic interaction criterion that is a function of the interlaminar strength values for each of the damage modes. Once debonding is initiated, the cohesive tractions transferred through the interface decrease linearly to zero according to the energy-based Benzeggagh-Kenane (BK) damage propagation criterion [30] that accounts for the dependence of the fracture energy dissipation on mode mixity. More details of this implementation can be found in [15, 19].

2.4. Model input parameters

In order to capture the influence of different environmental conditions on the ply behaviour, the input parameters of the constitutive models correspond to micromechanical characterization on the resin matrix and on the fibre/matrix interface performed at room temperature conditions (RT/DRY), as well as on samples conditioned up to saturation in an environmental chamber at 70^{o}C and 85% relative humidity (HOT/WET). The small size of the specimens required for micromechanical characterization leaded to a significantly faster water uptake as compared with the typical coupon size used in common practice, making the study of HOT/WET conditions very practical. A detailed explanation of the experimental micromechanical procedures carried in this work can be found in Rodriguez et al.[31, 32]. Their application to the particular case of the AS4/8552 material system under RT/DRY and HOT/WET conditions was covered in a previous work by the authors [15]. To summarize, the constituent material properties used in the present work are gathered in Table 1.

The set of thermoelastic properties for the AS4 carbon fibers was assumed to be independent of environmental conditions and is constituted by data provided by the material supplier or derived from the literature [1] using the Chamis rule of mixtures [33]. The polymer elastic modulus and compression strength (E_{m} and σ_{myc}) were measured by instrumented nanoindentation under RT/DRY and HOT/WET conditions, whereas its remaining properties, namely, fracture energy, tensile strength, Poisson ratio, coefficient of thermal expansion

(CTE) and internal friction angle ($\mathcal{G}_{\mathrm{m}}$, σ_{myt}, ν_{m}, α_{m} and β, respectively) were provided from the material supplier or taken from literature [17]. Under HOT/WET conditions, the polymer CTE was modified to include the effect of water absorption, according to the procedure described by the authors in [34]. It was assumed that the swelling of the polymer compensates for its shrinkage resulting from the curing process. Therefore, the CTE value results to be lower at HOT/WET conditions than under a RT/DRY environment.

Regarding the fiber/matrix interface, the mode II strength (τ_L) has been measured by means of push-in tests, and the mode I strength (τ_N) was assumed to be 2/3 of that value, as proposed by [35]. A parametric study led to the adoption of the friction coefficient μ=0.4 [15]. Finally, the interface fracture energies for mode I and mode II ($\mathcal{G}_{\mathrm{Ic}}$ and $\mathcal{G}_{\mathrm{IIc}}$) were set based on considerations with respect to reasonable values of the length of fracture process zones generated by fiber/matrix interface decohesion, and support of micromechanical observations. The values adopted for $\mathcal{G}_{\mathrm{Ic}}$ and $\mathcal{G}_{\mathrm{IIc}}$ are in line with those reported in the literature [36, 37].

Table 1: Properties of the AS4/8552 material constituents used in the FE simulations. Polymer fracture energy, tensile strength, Poisson ratio and internal friction angle are taken from [17]. Carbon fiber elastic properties are also extracted from [17]. Polymer elastic modulus and compression strength together with interface shear strength have been measured by instrumented nanoindentation. See [15] for further details.

AS4 carbon fiber properties							
	E_{f1} (GPa)	E_{f2} (GPa)	G_{f12} (GPa)	G_{f23} (GPa)	ν_{f12}	α_{f1} (K^{-1})	α_{f2} (K^{-1})
	231	12.97	11.28	4.45	0.3	-0.9e-6	7.2e-6
8552 epoxy matrix properties							
Condition	E_{m} (GPa)	ν_{m}	σ_{myt} (MPa)	β	σ_{myc}(MPa)	$\mathcal{G}_{\mathrm{m}}$ ($\mathrm{J/m^2}$)	α_{m} (K^{-1})
RT/DRY	5.07±0.3	0.35	121	29	176±17	100	52e-6
HOT/WET	4.28±0.2	0.35	104	29	152±08	100	1.5e-6
AS4/8552 fibre/matrix interface properties							
Condition	σ_N (MPa)	τ_T (MPa)	τ_L (MPa)	$\mathcal{G}_{\mathrm{Ic}}$ ($\mathrm{J/m^2}$)	$\mathcal{G}_{\mathrm{IIc}}$ ($\mathrm{J/m^2}$)	$\mathcal{G}_{\mathrm{IIIc}}$ ($\mathrm{J/m^2}$)	
RT/DRY	42	64	64±2.64	2	100	100	
HOT/WET	30	45	45±2.72	2	100	100	

3. Computational results, validation and discussion

3.1. Longitudinal compression stiffness

The reliability of the modeling approach regarding elastic response is assessed by correlating its results with reliable experimental values found in the literature [21]. The reported AS4/8552 ply longitudinal compression Young modulus, E_{1c}, has a low dependence on the environment, being $E_{1c} = 114$ GPa and $E_{1c} = 116$ GPa for RT/DRY and HOT/WET conditions, respectively. Since the composite elastic response is governed by the stiffness of the carbon fibers and those are not affected by moisture absorption, these experimental observations were expected. However, reported experimental E_{1c} values are markedly lower than their tensile counterparts, $E_{1t} \approx 136$ GPa (also fairly independent of environmental conditions). In principle, since E_1 is dominated by the elastic response of the carbon fiber, the origin of this difference can be attributed either to the initial fiber misalignment ϕ_0 or to different fiber behaviors in tension and compression.

To check the first hypothesis, a parametric study relating the value of E_{1c} and ϕ_0 is conducted using the single-fiber RVE model. Results are shown in Figure 4 for both RT/DRY and HOT/WET conditions. It can be observed that a similar relationship between both parameters is obtained for both environmental conditions when $\phi_0 < 2^o$. For larger values, the relationship between E_{1c} and ϕ_0 diverges due to the different polymer elasto-plastic properties for RT/DRY and HOT/WET conditions.

In order to estimate the longitudinal compression modulus of the homogenized ply, $E_{1c,ply}$, the fiber misalignment distribution of Figure 1 was considered in a method similar to the one followed by Barbero [38] to determine the ply compression strength, $X_{c,ply}$. Following this approach, the applied load function, $\widetilde{\sigma} = X_c(\phi_0)F(\phi_0)$, represents the effective stress on fibers that remain unbroken or un-kinked. This load function has a maximum that corresponds to the ply compression strength $X_{c,ply}$. Therefore, substitution of the misalignment sensitivity function $X_c(\phi_0)$ by the $E_{1c}(\phi_0)$ relationship of Figure 4 leads to the prediction of $E_{1c,ply}$ as the maximum of the curve $E_{1c}(\phi_0)F(\phi_0)$, hence obtaining $E_{1c,ply} = 130$ GPa and $E_{1c,ply} = 129$ GPa, for RT/DRY and HOT/WET conditions, respectively. These values still represent an important over-prediction of the ones obtained experimentally [21]. Therefore, it can be concluded that ϕ_0 has a minor influence on the longitudinal compression modulus of the

composite.

In view of this, and since the fiber properties used in the computational model were obtained under tensile loads, the difference between the ply longitudinal tension and compression moduli seems to derive mostly from the fiber elastic response rather than from geometrical imperfections. This idea has been pointed out by several authors, e.g. [39, 40], who stated that the longitudinal modulus of carbon fibers under tension (E_{ft}) and compression (E_{fc}) can be quite different. In particular, Mujika et al. [40] has shown that $E_{\mathrm{fc}}/E_{\mathrm{ft}} = 0.88$ for AS4 carbon fibers. The origin of this phenomenon is still not clear, hence this assumption needs to be considered carefully. High resolution images of PAN-based carbon fiber longitudinal and transverse sections have shown that there is a complex interlinking of layer planes both longitudinally and laterally [41]. The presence of misoriented crystallites, with respect to the fiber axis, could explain the lower value of the compression modulus compared to the tension one. However, more research work is required to understand the mechanical response of the carbon fiber inner structures.

Applying the correction factor proposed by Mujika et al. [40] to the modulus determined using Barbero's method [38] leads to set of ply compression modulus that are in good agreement with the ones experimentally obtained by Marlett et al. [21], as presented in Table 2.

3.2. Longitudinal compression strength

Although, the computation of the misalignment sensitivity function $X_{\mathrm{c}}(\phi_0)$ is not practical with the multi-fibre model (Figure 5), this RVE is able to capture the initiation of the fiber kinking damage process as well as showing some relevant post peak-load features. Following the notation used by Pimenta et al. [5], the fiber rotation angle (α) and band width (w) can be identified by the kinked RVE, as shown in Figure 5c. The predicted values ($\alpha \approx 14^o$ and $w \approx 120\,\mu\mathrm{m}$) are in good agreement with experimental data [42, 43, 44], as well as with numerical results published by other authors [14, 10, 12] for similar values of applied strain. In particular, Gutkin et al. [42] pointed out that the kink band width is in the order of 10-30 fiber diameters. Nevertheless, it is worth mentioning that the RVE approach is not suited to capture the propagation of damage but only its initiation. In fact, if periodic boundary conditions are used, the RVE corresponds to a UD ply region that is far away from the edges.

This means that the predicted kink-band angle, β, is zero as shown also by Gutkin et al. [12]. Fortunately, the does not influence the strength predictions since the kink-band angle only starts increasing after the peak load [5].

Unlike the multi-fibre RVE, the efficient 3D single-fiber RVE model cannot capture the aforementioned kink banding features but its predictions of the compression elastic modulus and of the kink load (X_c) match the ones obtained by the multi-fibre RVE for the same initial fiber misalignment (see Figure 5a). For the particular case of the AS4/8552 material, the fiber/matrix interface is weaker than the resin matrix, hence, the ply strength is governed by the fiber volume fraction and the initial misalignment. If this was not the case, the fiber distribution and inter-fiber spacing would control the onset of plastic deformation in the matrix and could govern the ply strength. In view of this, the efficient 3D single-fiber RVE can be used to perform parametric analyses and obtain $X_c(\phi_0)$ for the AS4/8552 material.

Modeling the fiber behavior as linear-elastic leads to unrealistic predictions of X_c for small values of the initial misalignment angle (roughly $0^o < \phi_0 < 1.0^o$), since under such conditions fiber crushing is bound to occur at lower loads than fiber kinking [12]. To account for this phenomenon in an approximated way, an isotropic continuum damage model available in the library of ABAQUS [19] was used. The authors infer that the fiber longitudinal compression modulus should be lower than the tensile one due to the morphology of the carbon fiber cross section [41]. However, the necessary fiber characterization results are not available. Hence, values found by Herráez et al. [45] for longitudinal fiber tension were used instead.

By using this approach, the sensitivity function $X_c(\phi_0)$ can finally be calculated for the different initial fiber misalignment values and both RT/DRY and HOT/WET environmental conditions. The numerical results are gathered in Figure 6a and compared to the analytically solutions implemented in LaRC04 [4] and developed by Pimenta et al. [10]. Remarkable correlation is obtained with LaRC04. The model of Pimenta et al. tends to overpredict X_c due to the assumption of an elastic-perfectly plastic matrix behavior. Both LaRC04 and present numerical approach adopt more realistic matrix plastic hardening response. Under RT/DRY conditions, the sensitivity function presents two different regions. Up to $\phi_0 = 1.0^o$, the failure mechanism is fiber crushing and the fracture process is governed by the fiber compression strength. For $\phi_0 > 1.0^o$, the initial fiber misalignment and matrix plasticity

controls the failure of the RVE, and therefore the failure occurs by kink band formation. In the case of HOT/WET conditions, the effect of fiber crushing is almost negligible ($\phi_0 < 0.5^o$). Nevertheless, under both conditions, the predicted values of $X_c(\phi_0)$ are clearly lower than the ones predicted by the analytic solution. This is due to the presence damageable fiber/matrix interface, whose failure triggers the onset of matrix plastic deformation, but also due to the matrix damage and carbon fiber anisotropy.

The actual ply compression strength $X_{c,ply}$, is predicted using the method developed by Barbero [38] introduced above. The nominal compression strengths of the composite ply are given by their maximum values of the applied load function, $\widetilde{\sigma} = X_c(\phi_0)F(\phi_0)$. The predicted load functions $\widetilde{\sigma}(\phi_0)$ for RT/DRY and HOT/WET conditions are shown in Figure 7. As presented in Table 2, the numerical results are in excellent agreement with experimentally-obtained values found in the literature [21] for both environmental conditions.

Table 2: Numerically-predicted vs. experimentally-obtained elastic constants and longitudinal compression strengths for a AS4/8552 ply.

	RT/DRY		HOT/WET	
Property	Micromechanics	Literature [21]	Micromechanics	Literature [21]
E_1 (GPa)	114	113.5±2	113	116.8±1
X_c (MPa)	1356	1441±43	1064	1065±30

3.3. Fiber kinking micromechanisms

With the purpose of studying the fiber kinking micromechanisms under different environments, the single-fiber configurations corresponding to the critical values of the initial fiber misalignment angle for RT/DRY and HOT/WET conditions, $\phi_0 = 1.31^\circ$ and $\phi_0 = 1.14^\circ$ respectively, are analyzed herein in great detail (see Figure 8). The HOT/WET case is used for illustration since similar mechanisms are captured for the RT/DRY condition.

Figure 8c shows the evolution of the interface scalar damage variable for progressive values of applied strain. With reference to the longitudinal and cross paths shown on the top of Figure 8c, the evolution of delamination span along the longitudinal and transverse direction (red triangles and black diamonds, respectively) and the matrix plasticity along the cross

section (blue squares) is monitored for increasing applied strains and graphically represented in Figure 8b. It can be observed that the kinking process is triggered by failure of the interface that initiates at the intersections of the fiber surface with the misalignment plane. In these stages ($0.008 < \epsilon < 0.01$), interface damage propagates along both longitudinal and circumferential paths, reducing the load transferred between the fiber and the matrix. This process, which is controlled by the interface energy release rate, continues until the onset of matrix damage ($\epsilon \approx 0.01$). At this point, longitudinal delamination is arrested and transverse delamination increases rapidly until the cross section becomes almost entirely damaged ($> 90\%$ of the total circumference perimeter) making the RVE unstable ($0.0105 < \epsilon < 0.0106$). This point corresponds to the maximum load supported by the RVE. During the post-peak($\epsilon > 0.0106$), the longitudinal delamination grows again and matrix undergoes severe plastic deformation.

To highlight the role of the fiber/matrix interface in the fiber kinking process, the RVE analyses were repeated using perfect interfaces. The stress-strain results corresponding to realistic and perfect interfaces are compared in Figure 8a for both environmental conditions. It can be concluded that interface failure triggers the collapse of the RVE, leading to important reductions of the maximum applied loads in comparison with analyses considering perfect interfaces. The load drop (22%) is specially important in the HOT/WET case because of the lower interface strength measured in this condition (see Table 1). Such influence of the interface was also reported by Madhukar et al. [46], who studied the effect of fiber/matrix interface strength in the longitudinal compression behaviour of UD composites.

It must be pointed that this analysis is only valid for the particular case of the AS4/8552 composite. In another material, with different matrix, fiber/matrix interface properties and fiber volume fraction, a different interaction of failure mechanisms might be observed.

4. Conclusion

A coupled experimental-computational micromechanics framework is proposed to simulate the longitudinal compression behaviour of unidirectional composite plies allowing the virtual investigation of environmental effects. The approach is based on the *in-situ* experimental characterization of the microconstituents. Using only material constituent properties,

the models developed are able to reproduce in detail the experimentally observed ply behavior and kinking mechanisms, although at a high computational cost. Simplified models are also proposed that provide still accurate results for the most important ply properties, compression elastic modulus and compression strength.

In the proposed approach, it was assumed that the major feature affecting fiber kinking is the initial fiber misalignment generated during composite manufacturing. Other manufacturing defects have been demonstrated by other authors to have effects on the compression strength, but they were considered here to be minor and not analyzed. Moreover, The experimental measurements of this property to which the present results are correlated are likely to be affected by the experimental set-up, by the sample size and geometry, among other factors. In view of this, the present virtual test approach can be understood to provide the upper limits of the ranges of variability of the measured properties.

In summary, this paper proposes a virtual ply characterization methodology based on reliable properties of the microconstituents, aimed to replace the physical experiments, at least for material screening purposes. These virtual tests provide full control of the composite microstructure and constituent properties, allowing microstructural optimization to be performed in the future. Moreover, the computational approach allows the simulation of complex stress states, not possible to be applied experimentally. The importance of some micromechanical parameters, such as fiber distribution, cohesive-frictional fiber/matrix interface properties, fiber behaviour under tension and compression, still need to be assessed by future research.

Acknowledgments

This work was conducted under financial support of AIRBUS SAS through the project SIMSCREEN (Simulation for Screening Composite Materials Properties). Additionally, C.S. Lopes acknowledges the Spanish Ministry of Economy and Competitiveness through the *Ramón y Cajal* program (grant RYC-2013-14271). The collaboration with NASA Langley Research Center in some aspects of this research is also acknowledged.

References

[1] M. Hinton, A. Kaddour, P. Soden, A further assessment of the predictive capabilities of current failure theories for composite laminates: comparison with experimental evidence, Composites Science and Technology 64 (2004) 549–588.

[2] B. Budiansky, N. A. Fleck, Compressive kinking of fiber composites : A topical review, Appl Mech Rev 47 (1994) 246–250.

[3] P. Berbinau, C. Soutis, P. Goutas, P. Curtis, Effect of off-axis ply orientation on 0º-fibre microbuckling, Composites Part A: Applied Science and Manufacturing 30 (1999) 1197–1207.

[4] S. T. Pinho, C. G. Dávila, P. P. Camanho, L. Iannucci, P. Robinson, Failure Models and Criteria for FRP Under In-Plane or Three-Dimensional Stress States Including Shear Non-linearity, Technical Report February, 2005.

[5] S. Pimenta, R. Gutkin, S. T. Pinho, P. Robinson, A micromechanical model for kink-band formation: Part I-Experimental study and numerical modelling, Composites Science and Technology 69 (2009) 948–955.

[6] S. L. Bazhenov, A. M. Kuperman, E. S. Zelenskii, A. A. Berlin, Compression failure of unidirectional glass-fibre-reinforced plastics, Composites Science and Technology 45 (1992) 201–208.

[7] W. V. Liebig, K. Schulte, B. Fiedler, Hierarchical analysis of the degradation of fibre-reinforced polymers under the presence of void imperfections, Philosophical Transactions of the Royal Society A: Mathematical, Physical and Engineering Sciences 374 (2016).

[8] C. Soutis, D. Turkmen, Moisture and Temperature Effects of the Compressive Failure of CFRP Unidirectional Laminates, Journal of Composite Materials 31 (1997) 832–849.

[9] S. Narayanan, L. S. Schadler, Mechanisms of kink-band formation in graphite/epoxy composites: A micromechanical experimental study, Composites Science and Technology 59 (1999) 2201–2213.

[10] S. Pimenta, R. Gutkin, S. T. Pinho, P. Robinson, A micromechanical model for kink-band formation: Part II-Analytical modelling, Composites Science and Technology 69 (2009) 956–964.

[11] T. Vogler, S. Kyriakides, Initiation and axial propagation of kink bands in fiber composites, Acta Materialia 45 (1997) 2443–2454.

[12] R. Gutkin, S. T. Pinho, P. Robinson, P. Curtis, Micro-mechanical modelling of shear-driven fibre compressive failure and of fibre kinking for failure envelope generation in CFRP laminates, Composites Science and Technology 70 (2010) 1214–1222.

[13] R. Gutkin, S. T. Pinho, P. Robinson, P. Curtis, A finite fracture mechanics formulation to predict fibre kinking and splitting in CFRP under combined longitudinal compression and in-plane shear, Mechanics of Materials 43 (2011) 730–739.

[14] X. Bai, M. A. Bessa, A. Melro, P. P. Camanho, L. Guo, W. K. Liu, High-fidelity micro-scale modeling of the thermo-visco-plastic behavior of carbon fiber polymer matrix composites, Composite Structures 134 (2015) 132–141.

[15] F. Naya, C. González, C. S. Lopes, S. Van der Veen, F. Pons, Computational micromechanics of the transverse and shear behavior of unidirectional fiber reinforced polymers including environmental effects, Composites Part A: Applied Science and Manufacturing 92 (2017) 146–157.

[16] L. P. Canal, C. González, J. Segurado, J. LLorca, Intraply fracture of fiber-reinforced composites: Microscopic mechanisms and modeling, Composites Science and Technology 72 (2012) 1223–1232.

[17] M. Herráez, D. Mora, F. Naya, C. S. Lopes, C. González, J. LLorca, Transverse cracking of cross-ply laminates: A computational micromechanics perspective, Composites Science and Technology 110 (2015) 196–204.

[18] D. Ashouri Vajari, C. González, J. Llorca, B. N. Legarth, A numerical study of the influence of microvoids in the transverse mechanical response of unidirectional composites, Composites Science and Technology 97 (2014) 46–54.

[19] Dassault Systèmes, Abaqus 6.13 Documentation, 2013.

[20] T. Vaughan, C. McCarthy, A combined experimentalnumerical approach for generating statistically equivalent fibre distributions for high strength laminated composite materials, Composites Science and Technology 70 (2010) 291–297.

[21] K. Marlett, Y. Ng, J. Tomblin, E. Hooper, NCAMP Test Report: CAM-RP-2010-002 Rev A, Technical Report, National Institute for Aviation Research, 2011.

[22] M. W. Czabaj, M. L. Riccio, W. W. Whitacre, Numerical reconstruction of graphite/epoxy composite microstructure based on sub-micron resolution X-ray computed tomography, Composites Science and Technology 105 (2014) 174–182.

[23] S. Yurgartis, Measurement of small angle fiber misalignments in continuous fiber composites, Composites Science and Technology 30 (1987) 279–293.

[24] J. Lee, C. Soutis, A study on the compressive strength of thick carbon fibre-epoxy laminates, Composites Science and Technology 67 (2007) 2015–2026.

[25] C. González, J. LLorca, Mechanical behavior of unidirectional fiber-reinforced polymers under transverse compression: Microscopic mechanisms and modeling, Composites Science and Technology 67 (2007) 2795–2806.

[26] J. Segurado, J. LLorca, A numerical approximation to the elastic properties of sphere-reinforced composites, Journal of the Mechanics and Physics of Solids 50 (2002) 2107–2121.

[27] D. C. Drucker, W. Prager, Soil mechanics and plastic analysis for limit design, Quarterly of Applied Mathematics 10 (1952) 157–165.

[28] J. Lubliner, X. Oliver, S. Oller, E. Oñate, A plastic-damage model for concrete, International Journal of Solids and Structures 25 (1989) 299–326.

[29] J. Lee, G. L. Fenves, Plastic-Damage Model for Cyclic Loading of Concrete Structures, Journal of Engineering Mechanics 124 (1998) 892–900.

[30] M. L. Benzeggagh, M. Kenane, Measurement of mixed-mode delamination fracture toughness of unidirectional glass/epoxy composites with mixed-mode bending apparatus, Composites Science and Technology 56 (1996) 439–449.

[31] M. Rodríguez, J. M. Molina-Aldareguía, C. González, J. LLorca, Determination of the mechanical properties of amorphous materials through instrumented nanoindentation, Acta Materialia 60 (2012) 3953–3964.

[32] M. Rodríguez, J. M. Molina-Aldareguía, C. González, J. LLorca, A methodology to measure the interface shear strength by means of the fiber push-in test, Composites Science and Technology 72 (2012) 1924–1932.

[33] C. Chamis, Mechanics of Composite Materials: Past, Present, and Future, ASTM 11 (1989).

[34] F. Naya, J. M. Molina-Aldareguía, C. S. Lopes, C. González, J. LLorca, Interface Characterization in Fiber-Reinforced PolymerMatrix Composites, JOM 69 (2017) 13–21.

[35] S. Ogihara, J. Koyanagi, Investigation of combined stress state failure criterion for glass fiber/epoxy interface by the cruciform specimen method, Composites Science and Technology 70 (2010) 143–150.

[36] A. Melro, P. P. Camanho, F. Andrade Pires, S. T. Pinho, Micromechanical analysis of polymer composites reinforced by unidirectional fibres: Part II Micromechanical analyses, International Journal of Solids and Structures 50 (2013) 1906–1915.

[37] T. Vaughan, C. McCarthy, A micromechanical study on the effect of intra-ply properties on transverse shear fracture in fibre reinforced composites, Composites Part A: Applied Science and Manufacturing 42 (2011) 1217–1228.

[38] E. J. Barbero, Prediction of Compression Strength of Unidirectional Polymer Matrix Composites, Journal of Composite Materials 32 (1998) 483–502.

[39] N. Oya, D. J. Johnson, Longitudinal compressive behaviour and microstructure of PAN-based carbon fibres, Carbon 39 (2001) 635–645.

[40] F. Mujika, N. Carbajal, A. Arrese, I. Mondragon, Determination of tensile and compressive moduli by flexural tests, Polymer Testing 25 (2006) 766–771.

[41] S. C. Bennett, D. J. Johnson, W. Johnson, Strength-structure relationships in PAN-based carbon fibres, Journal of Materials Science 18 (1983) 3337–3347.

[42] R. Gutkin, S. T. Pinho, P. Robinson, P. T. Curtis, On the transition from shear-driven fibre compressive failure to fibre kinking in notched CFRP laminates under longitudinal compression, Composites Science and Technology 70 (2010) 1223–1231.

[43] P. M. Jelf, N. A. Fleck, The failure of composite tubes due to combined compression and torsion, Journal of Materials Science 29 (1994) 3080–3084.

[44] S. T. Pinho, P. Robinson, L. Iannucci, Fracture toughness of the tensile and compressive fibre failure modes in laminated composites, Composites Science and Technology 66 (2006) 2069–2079.

[45] M. Herráez, A. Fernández, C. S. Lopes, C. González, Strength and toughness of structural fibres for composite material reinforcement, Philosophical Transactions of the Royal Society of London. Series A, Containing Papers of Mathematical or Physical Character 374 (2016) 1–12.

[46] M. S. Madhukar, L. T. Drzal, Fiber-Matrix Adhesion and Its Effect on Composite Mechanical Properties. III. Longitudinal (0°) Compressive Properties of Graphite/Epoxy Composites, Journal of Composite Materials 25 (1991) 932 –957.

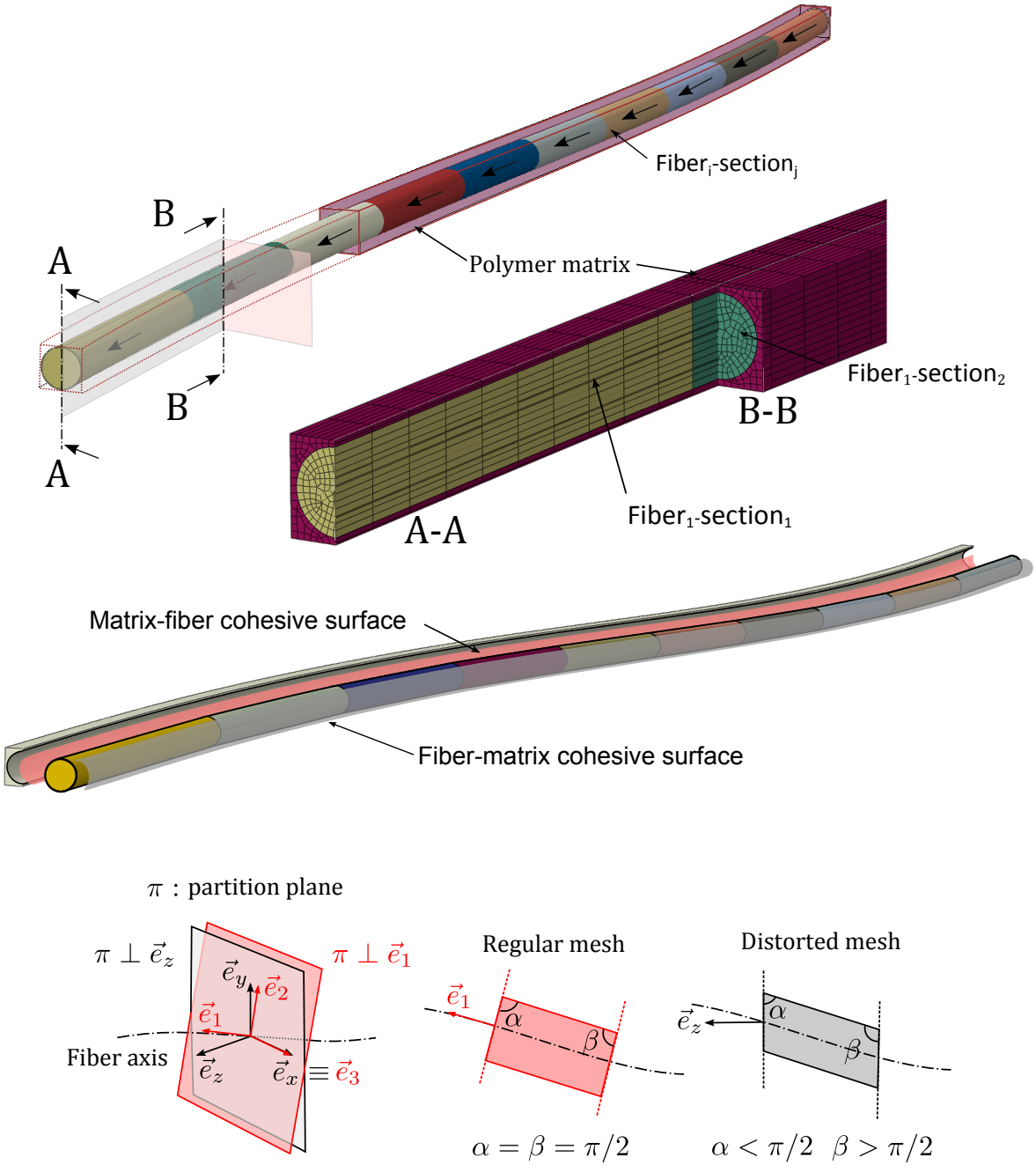

Figure 3: Single-fibre FE model used in the simulation of longitudinal compression of a AS4/8552 ply (each color represents one section; arrows show the orientation of the fibers) including the geometry partition strategy used to orient the fibers and provide a regular mesh (distorted mesh resulting from using planes perpendicular to the global z axis is shown for comparison).

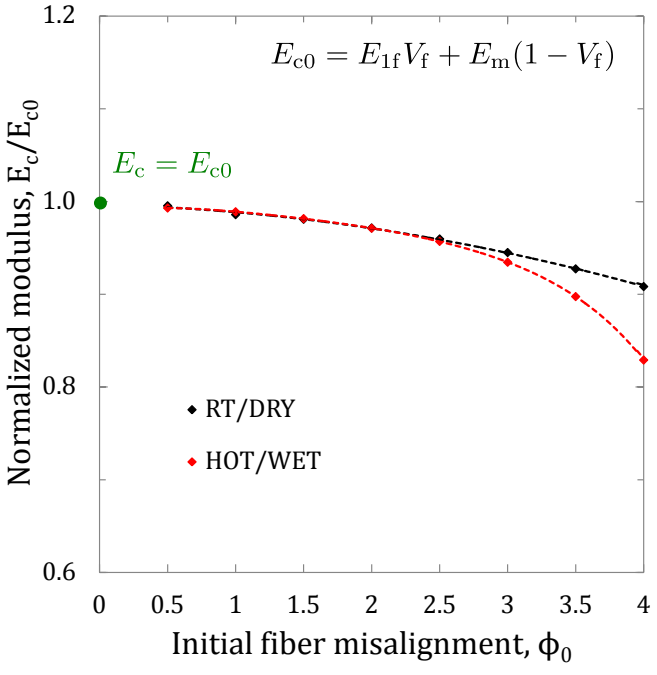

Figure 4: Predicted AS4/8552 longitudinal compression modulus evolution ($E_c(\phi_0)$), for different initial fiber misalignments (ϕ_0) under RT/DRY and HOT/WET conditions. Linear and nonlinear regions are pointed out together with the corresponding fitting equations.

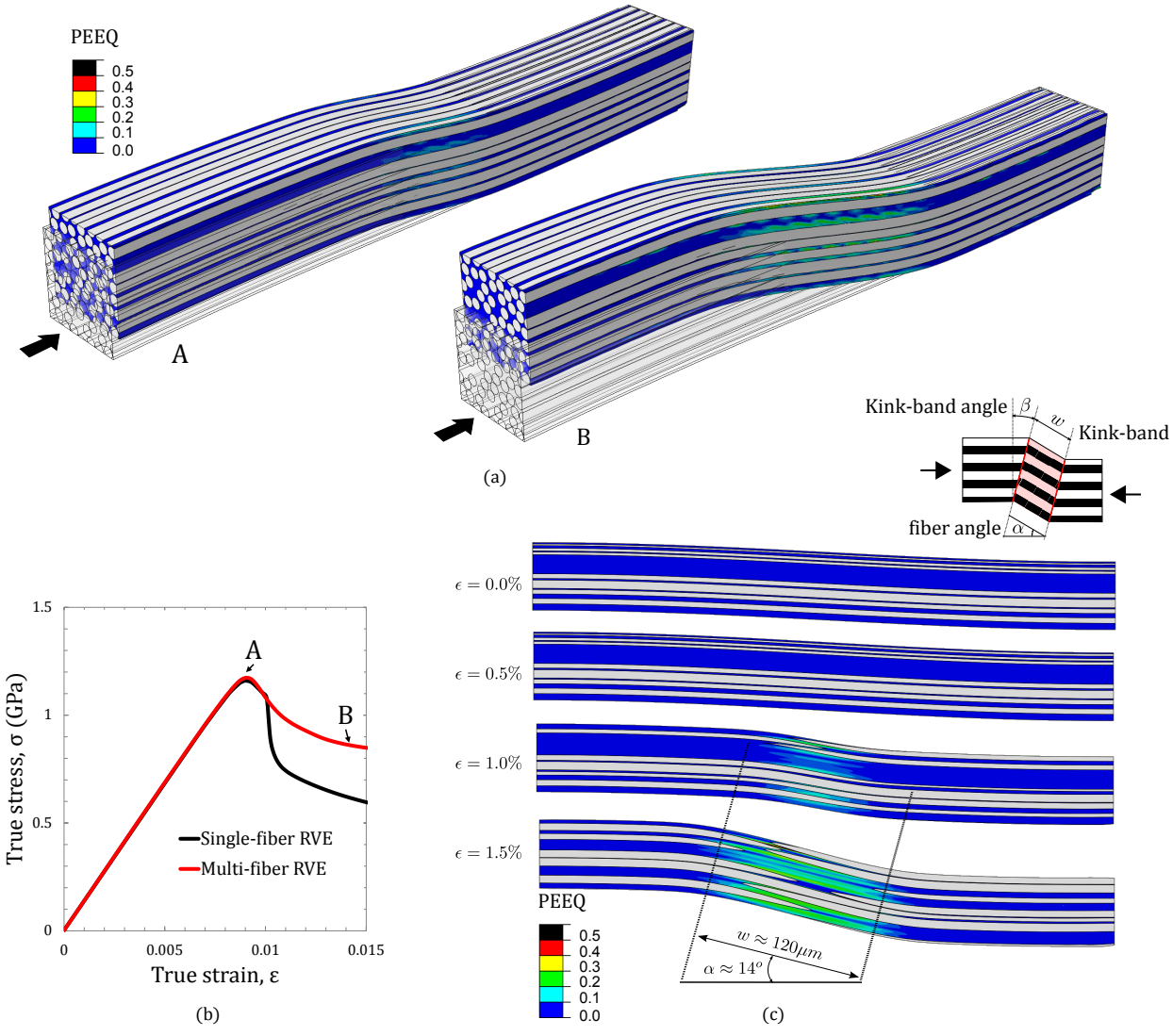

Figure 5: Predicted kink-band development in AS4/8552 under RT/DRY conditions and pure longitudinal compression: a) Plastic equivalent strain (PEEQ) at two load states: A - kink-band initiation corresponding to peak load; and B - fully developed kink-band; b) Stress-strain curve - Comparison between complex and simplified RVE for the same initial fiber misalignment, $\phi_0 = 3^o$; c) Plastic equivalent strain (PEEQ) evolution with prediction of kink-band width and fiber angle α.

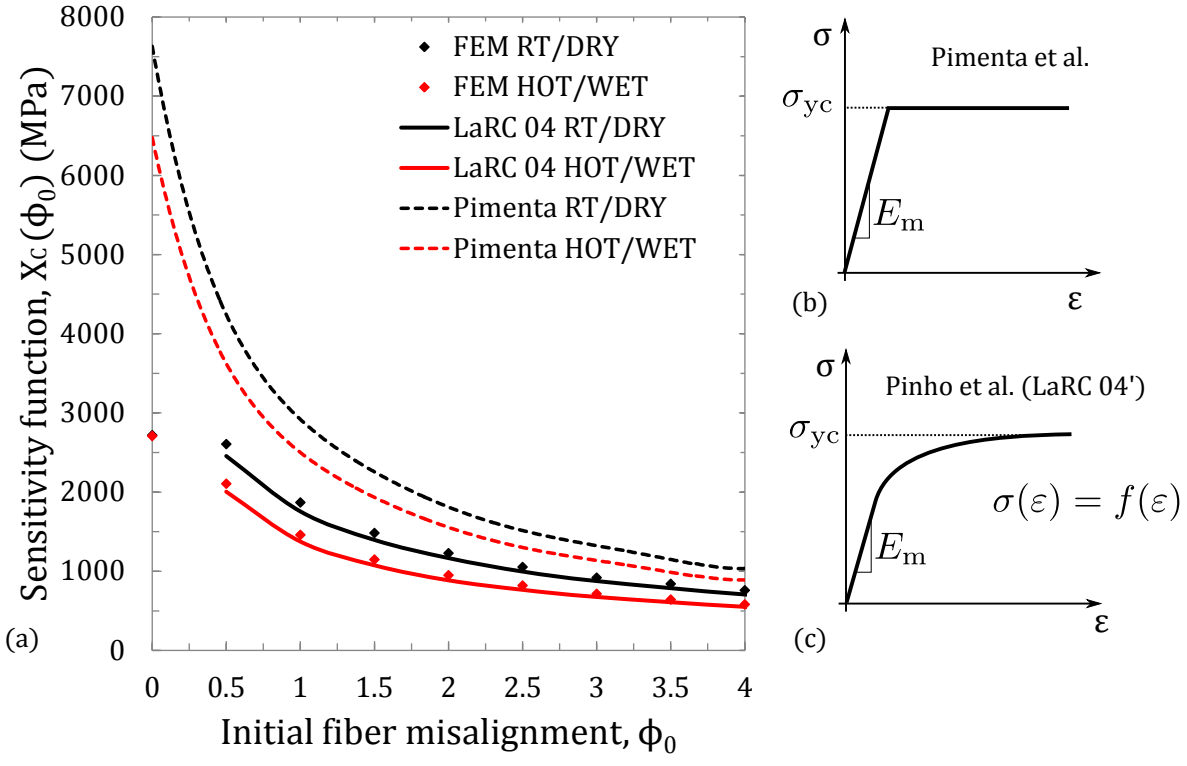

Figure 6: a) Predicted AS4/8552 ply compression strength evolution ($X_c(\phi_0)$), for different initial fiber misalignment (ϕ_0) under RT/DRY and HOT/WET conditions. Comparison between present FE simulations and analytical solutions implemented in LaRC04 [4] and developed by Pimenta et al. [10]. Schematic representation of the matrix elasto-plastic response adopted by both Pimenta's and LaRC analytical solutions is shown in (b) and (c) respectively.

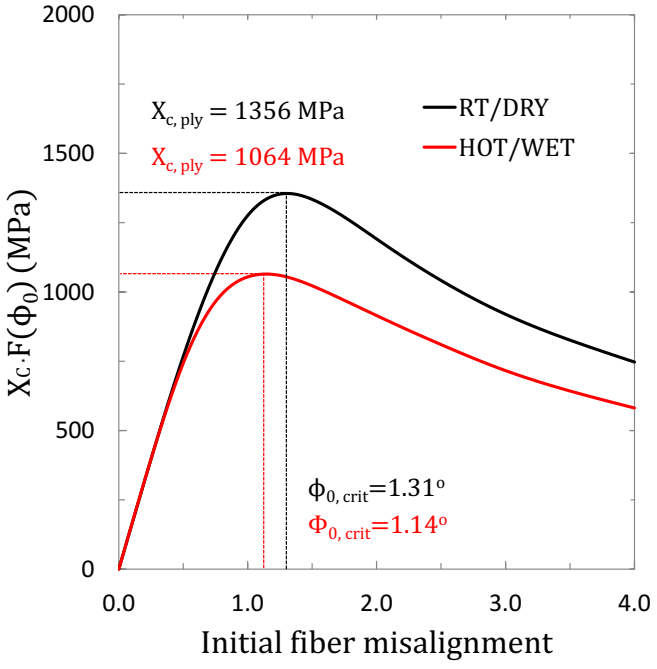

Figure 7: Barbero's load function $\widetilde{\sigma}(\phi_0)$ predicted for AS4/8552 under RT/DRY and HOT/WET conditions.

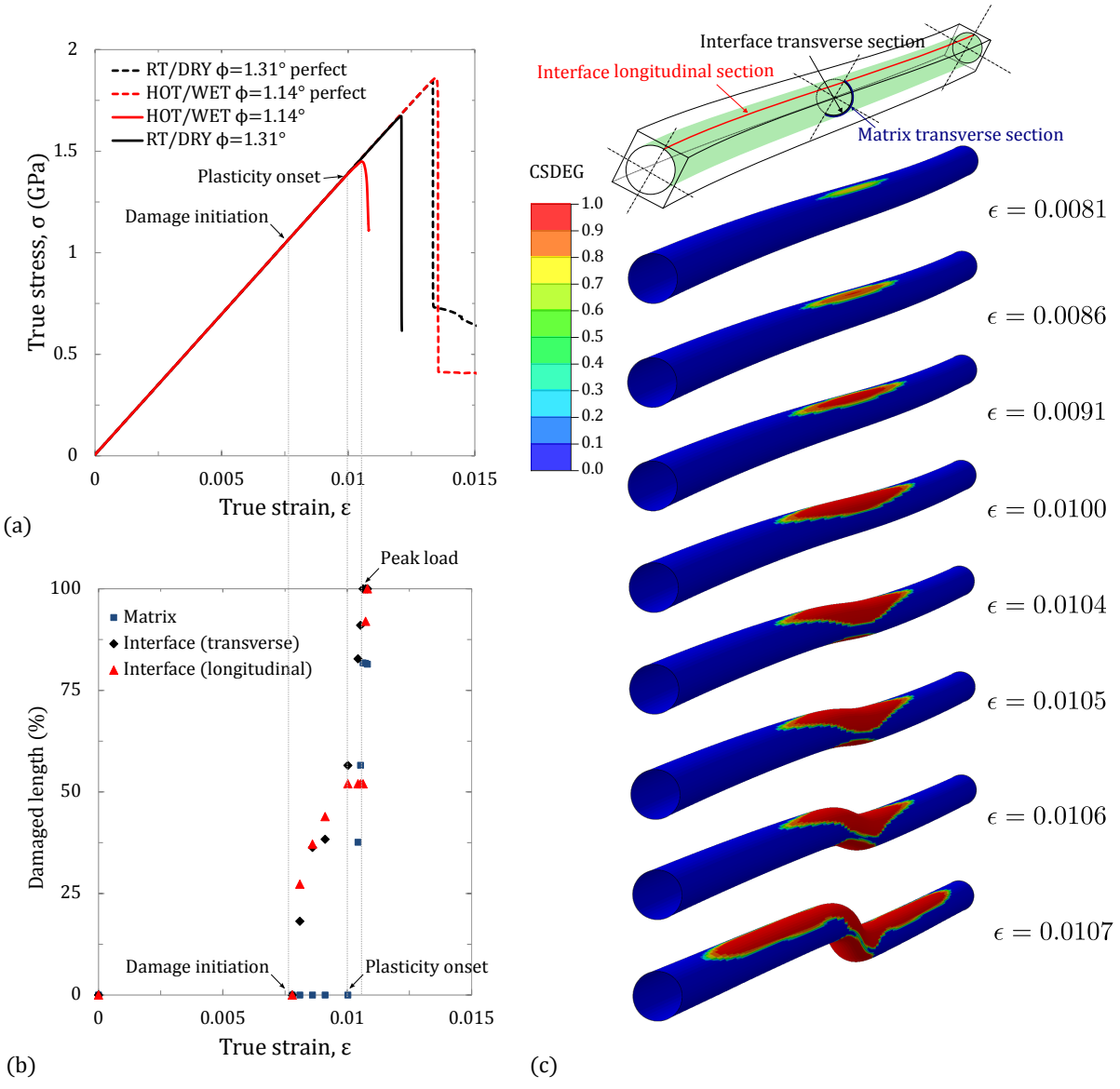

Figure 8: a) Predicted AS4/8552 ply compression strength for critical initial fiber misalignment (ϕ_0) under RT/DRY and HOT/WET conditions. Comparison between realistic and perfect interface cases; b) Evolution of interface damage (along fiber direction and transverse sections perimeter) and matrix plasticity along transverse section perimeter for the case of real interface under HOT/WET conditions; c) Progressive increase of interface damage with applied compression load for the case of real interface under HOT/WET conditions.